Original Paper

Eletrônica de Potência
Open Journal of Power Electronics

Received July 31, 2024; accepted October 28, 2024; Date of publication November 11, 2024.
The review of this paper was arranged by Associate Editor Margarita Norambuena and Editor-in-Chief Heverton A. Pereira.

Digital Object Identifier http://doi.org/10.18618/REP.e202446

Iterative Methods for Nonlinear Systems Applied to Grid Impedance Estimation: A Comparative Study

Jefferson R. P. de Assis[1], Andréia da S. Gomes[2], Hugo M. T. C. Gomes[2], Fabiano F. Costa[2], Wellington F. Felipe[3], Maurício B. de R. Corrêa[4], Darlan A. Fernandes[3].

[1]Federal University of Campina Grande, Department of Electrical Engineering, Campina Grande – PB, Brazil.
[2]Federal University of Bahia, Department of Electrical Engineering, Salvador – BA, Brazil.
[3]Federal University of Paraíba, Department of Electrical Engineering, João Pessoa – PB, Brazil.
[4]Federal University of Alagoas, Institute of Computing, Maceió – AL, Brazil.

e-mail: jefferson.assis@ee.ufcg.edu.br; andreiagomes@ufba.br; hugo.cotrim@ufba.br; fabiano.costa@ufba.br; wellington.felipe@cear.ufpb.br; mauricio@ic.ufal.br; darlan@cear.ufpb.br

ABSTRACT In this work, a comparative study is presented to evaluate the performance of iterative methods to solve nonlinear systems applied to grid impedance estimation. The iterative methods of Newton-Raphson, Potra-Pták, and Chun were embedded in the control system of a three-phase inverter supported by a photovoltaic plant connected to the grid. The adopted impedance estimation technique consists of successive variation of the power injected into the grid, more precisely, at three different levels. The voltage and current amplitudes at the point of common coupling (PCC) are monitored and serve as input for the iterative methods, which, after processing them, provide an estimate of the grid impedance. To compare the performance between the methods, the following merit figures were listed: execution time, number of iterations required to deliver the estimates, percentage error, efficiency index, computational efficiency, computational efficiency index, and stability of the iterative method. The results presented were obtained through real-time simulations. From that, it was possible to conclude about the method with the best performance, thus contributing to greater assertiveness on the part of designers when choosing the most efficient iterative method to be embedded in a microcontroller for grid impedance estimation purposes.

KEYWORDS Chun method, comparative analysis, grid impedance estimation, iterative methods, Newton-Raphson method, nonlinear systems, Potra-Pták method.

I. INTRODUCTION

In April 2023, the Group of Seven (G7) pledged to further and encourage a global green transition, collaborating to transform their economies and reach net zero greenhouse gas (GHG) emissions by 2050 [1]. Currently, severe climatic and environmental changes, along with growing concerns about the future supply of non-renewable energy resources, underscore the urgency of transitioning to predominantly green energy systems [2].

These facts encourage the increasing use of renewable energy sources which, when combined with the electrification of transport, brings an increase in the number of power electronic converters connected to electrical energy distribution grids. Therefore, investigation of phenomena related to the converter-grid interaction becomes essential to increase the reliability and efficiency of these systems.

The first record on the analysis of the interaction between the output impedance of a converter and the impedance of the grid to which it is connected was presented in the 1970s by [3], where a case covering dc-dc converters was investigated. In the 1990s, the approach recorded in [3] was generalized for application to dc-ac systems [4], [5].

In the twentieth century, undesirable behavior was observed in the converter-grid interaction. This fact was recorded in [6], where it was concluded that the connection of distributed generation sources with the distribution grid of an utility can lead to system instability if they are not properly designed. More precisely, a high grid impedance can cause system stability problems [7].

Given this context, the need to know the impedances involved in the converter-grid interaction arose, which led to the so-called impedance estimation techniques. The main applications of impedance estimation are grid characterization, anti-islanding detection, filter resonance prevention, adaptive control, and stability analysis [8].

In recent years, several impedance estimation techniques have been proposed and recorded in the specialized literature. In [9] an online event-based grid impedance estimation technique was proposed for grid-connected inverters. The strategy consists of imposing variations in the inverter output power and monitoring variations of the positive sequence amplitude point common coupling (PCC) voltage. When used in the context of impedance estimation techniques, the

term *online* means that the parameter estimation is performed with the system in full operation.

It was in [10] that the estimation of the X/R relationship of the grid was proposed to determine a virtual impedance in the control of the converter. The main objective of this action is to improve the control of the power flow of the grid-forming converters. In [11], an impedance estimation technique was proposed based on variations in power levels injected by an inverter connected to the grid, changes in PCC voltages and currents were monitored and used as input for the numerical method of Newton-Raphson, resulting in the estimated RL values of the grid.

An approach for estimating grid impedance based on a pulsed signal injection (PSI) technique and an impedance modeling tool in a low-voltage grid with parallel connected converters was presented in [12]. In [13], the impedance of the grid to which an inverter was connected and estimated by inserting a pseudorandom binary sequence (PRBS) directly into the control system. The responses to the disturbances were recorded and analytically manipulated to estimate the parameters.

Recently, a technique for estimating the grid impedance in the reference frame dq was presented in [14]. The strategy is based on the interpolated discrete Fourier transform to extract the phase angle of the grid and then estimate the parameters RL. The results indicate that the method was able to estimate the grid impedance accurately even at lower frequencies. In [15], a method based on zero-sequence voltage injection was proposed to estimate the grid impedance. Basically, it was proposed to inject a third harmonic before space vector pulse width modulation, in order to generate sequence voltage zero on the output side of the inverter. Then, the voltage response at the PCC is measured to estimate the grid impedance.

By knowing that currently the computational and storage power of microcontrollers is increasing every year, the embedded and dedicated algorithms for estimating grid impedance must be optimized to provide increasingly faster control system decision-making, in addition, the precision of estimates must be the best possible, as mistaken estimates will result in equally erroneous decision making by the control system. This fact brings to light an opportunity to contribute with the algorithm performances dedicated to grid impedance estimation.

In [16] a comparison was made between two iterative methods applied to grid impedance estimation, where three merit figures were adopted to carry out the analysis, which were: the execution time, the number of iterations necessary to the delivery of estimates and the percentage error.

In this work, an analysis of the performance of iterative methods for solving nonlinear systems applied to the estimation of the impedance of the grid is presented. Here, the Newton-Raphson, Potra-Pták and Chun methods had their performances compared based on the following figures of merit: execution time, number of iterations required to deliver the estimates, percentage error, efficiency index, computational efficiency, computational efficiency index, and stability of the iterative method. The objective of this comparative study is to conclude on the most appropriate iterative method to be embedded and dedicated to grid impedance estimation in a microcontroller, contributing to increasing the reliability of converters connected to the grid.

To achieve the proposed objective, the iterative methods to be analyzed were embedded in the control system of a three-phase inverter supported by a photovoltaic plant connected to the grid. The performance of each method was recorded for each of the merit figures listed using real-time simulations. From the results obtained, it was possible to conclude that it is the most efficient iterative method.

The organization of this work was defined as described in the following. Section II presents the grid impedance estimation method used, highlighting the step-by-step process for obtaining the estimated parameters. In Section III, the iterative methods to be compared are mathematically described, and in addition, each of the figures of merit listed is properly defined. In Section IV, the following are presented: the photovoltaic system connected to the grid via a three-phase inverter, the real-time validation platform, and the results observed for the performance of each iterative method, being duly discussed. Finally, Section V summarizes the general conclusions of the work.

II. GRID IMPEDANCE ESTIMATION METHOD

Fig. 1 illustrates a generic grid-connected distributed generation system (DGS). In this, a DGS injects current $I_k\angle\varphi_k$ into a grid represented by a voltage source $V_{gk}\angle\delta_k$ of impedance $Z_{grid} = R_g + j\omega L_g$, which being R_g, ω and L_g, respectively, the resistance, the nominal frequency and the inductance of the grid. The voltage in the PCC is represented by $V_k\angle 0°$. The subscript k identifies different levels of power that the DGS can inject into the grid.

Observing the variables presented in Fig. 1 one can write:

$$V_{gk}\angle\delta_k = V_k - (R_g + j\omega L_g)I_k\angle\varphi_k \ . \tag{1}$$

Writing $V_{gk}\angle\delta_k$ and $I_k\angle\varphi_k$ in rectangular form:

$$V_{gk}\angle\delta_k = V_{gk}\cos\delta_k + jV_{gk}\sin\delta_k = V_{gkx} + jV_{gky} \ . \tag{2}$$

$$I_k\angle\varphi_k = I_k\cos\varphi_k + jI_k\sin\varphi_k = I_{kx} + jI_{ky} \ . \tag{3}$$

The subscripts x and y denote the real and imaginary components, respectively. Compared (1) with (2) and replacing

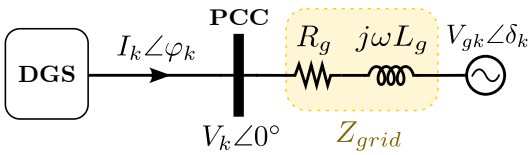

FIGURE 1. Generic grid-connected distributed generation system.

(3) in (1), we obtain the following:

$$\begin{aligned} V_{gkx} + jV_{gky} &= V_k - (R_g + j\omega L_g)(I_{kx} + jI_{ky}) \\ &= V_k - R_g I_{kx} - jR_g I_{ky} - j\omega L_g I_{kx} + \omega L_g I_{ky} \\ &= \underbrace{V_k - R_g I_{kx} + \omega L_g I_{ky}}_{Real} \underbrace{-j(R_g I_{ky} + \omega L_g I_{kx})}_{Imaginary} . \end{aligned} \tag{4}$$

When comparing the sides of (4), we note that:

$$\begin{cases} V_{gkx} = V_k - R_g I_{kx} + \omega L_g I_{ky} \\ V_{gky} = -R_g I_{ky} - \omega L_g I_{kx} \end{cases} . \tag{5}$$

Considering three different possible levels of power injected into the grid by DGS, system (5) becomes:

$$\begin{cases} V_{g1x} = V_1 - R_g I_{1x} + \omega L_g I_{1y} \\ V_{g1y} = -R_g I_{1y} - \omega L_g I_{1x} \\ V_{g2x} = V_2 - R_g I_{2x} + \omega L_g I_{2y} \\ V_{g2y} = -R_g I_{2y} - \omega L_g I_{2x} \\ V_{g3x} = V_3 - R_g I_{3x} + \omega L_g I_{3y} \\ V_{g3y} = -R_g I_{3y} - \omega L_g I_{3x} \end{cases} . \tag{6}$$

The instantaneous decomposition technique into sequence components (IDSC) presented in [17] has as input the measurements of the voltage at the PCC and the current injected into the grid by the DGS. The result of applying this algorithm are estimates of the voltage amplitude in the PCC (V_k) and the amplitude (I_k) and phase (φ_k) of the current injected into the grid. Consequently, for each of the three possible different levels of power injected, V_1, V_2, V_3, I_{1x}, I_{1y}, I_{2x}, I_{2y}, I_{3x} and I_{3y} are known. Thus, the system (6) has six equations and eight incognitos: V_{g1x}, V_{g1y}, V_{g2x}, V_{g2y}, V_{g3x}, V_{g3y}, R_g and L_g.

It is reasonable to assume that the grid voltage amplitude (V_{gk}) does not experience significant variations during the three different power levels injected by the DGS, i.e. $V_{g1} = V_{g2} = V_{g3}$. In other words, it can be considered that the phasor module $V_{gk}\angle\delta_k$ does not change during the application of the grid impedance estimation method. Knowing that the module of $V_{gk}\angle\delta_k$ is given by:

$$|V_{gk}\angle\delta_k| = V_{gk} = V_{gkx}^2 + V_{gky}^2 , \tag{7}$$

it can be expressed as:

$$V_{g1x}^2 + V_{g1y}^2 = V_{g2x}^2 + V_{g2y}^2 \tag{8}$$

$$V_{g2x}^2 + V_{g2y}^2 = V_{g3x}^2 + V_{g3y}^2 . \tag{9}$$

The system (6) combined with (8) and (9) form:

$$\begin{cases} V_{g1x} = V_1 - R_g I_{1x} + \omega L_g I_{1y} \\ V_{g1y} = -R_g I_{1y} - \omega L_g I_{1x} \\ V_{g2x} = V_2 - R_g I_{2x} + \omega L_g I_{2y} \\ V_{g2y} = -R_g I_{2y} - \omega L_g I_{2x} \\ V_{g3x} = V_3 - R_g I_{3x} + \omega L_g I_{3y} \\ V_{g3y} = -R_g I_{3y} - \omega L_g I_{3x} \\ V_{g1x}^2 + V_{g1y}^2 = V_{g2x}^2 + V_{g2y}^2 \\ V_{g2x}^2 + V_{g2y}^2 = V_{g3x}^2 + V_{g3y}^2 \end{cases} . \tag{10}$$

Note that the nonlinear system of equations (10) is formed by eight equations and eight unknown variables and can be solved with a single solution. In this work, the grid impedance estimation technique presented by [11] was adopted. The strategy consists of imposing via the control system that the DGS injects three different power levels successively, where during time range of each power level, the voltage and current amplitudes at the PCC and the current phase angle injected into the grid are captured via IDSC. At the end of the duration of the three programmed power levels, the captured information serves as input for an iterative method to solve nonlinear equation systems, which, when solving system (10), results in the estimated impedance of the grid. Fig. 2 illustrates the grid impedance estimation process adopted.

At this point, it is worth noting that the scope of this work is restricted to evaluating the performance of iterative methods for nonlinear systems applied to grid impedance estimation.

III. ITERATIVE METHODS FOR NONLINEAR SYSTEMS

It is known that the behavior of most physical phenomena is nonlinear in nature. However, the analytical solution of these problems is often too extensive or even impossible depending on the complexity of the problem. [18].

Advances in computer processing power have enabled iterative methods to be consolidated as a viable, fast, and efficient alternative to solve nonlinear problems [19], [20].

A generalized nonlinear system of equations can be written as:

$$\begin{cases} f_1(x_1, x_2, \ldots, x_n) = 0 \\ f_2(x_1, x_2, \ldots, x_n) = 0 \\ \vdots \\ f_n(x_1, x_2, \ldots, x_n) = 0 \end{cases} \Rightarrow F(\mathbf{x}) = \mathbf{0} , \tag{11}$$

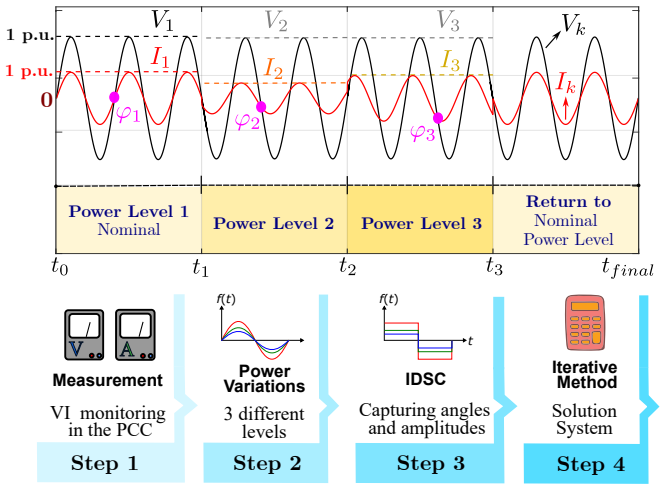

FIGURE 2. Grid impedance estimation method - Step by Step.

$f_1, \cdots, f_n$ n being nonlinear functions of n variables and F a vector function in $\mathbf{x} \in \mathbb{R}^n$.

Solving this system consists of determining the $\mathbf{x}$ that satisfy (11). In general, it is possible to obtain approximate solutions using iterative methods such as $\mathbf{x}_{k+1} = \Phi(\mathbf{x}_k)$, where $\mathbf{x}_k$ is the approximate solution in the k-th iteration.

The iterative methods covered in this work are of the type $\mathbf{x}_{k+1} = \Phi(\mathbf{x}_k)$. These result in a sequence of vectors $\{\mathbf{x}_k\}_{k=0}^{\infty}$, with k being the index of the step (or iteration) and $\mathbf{x}_k$ the approximation of the solution in the k-th iteration. From an initial estimate $\mathbf{x}_0$, this sequence may diverge or converge to a root $\mathbf{x}^{*,i}$ of the system $F(\mathbf{x}) = \mathbf{0}$ [21].

A. NEWTON-RAPHSON METHOD

The Newton-Raphson method boils down to the solution of:

$$\mathbf{x}_{k+1} = \mathbf{x}_k - J^{-1}(\mathbf{x}_k) F(\mathbf{x}_k) \ , \tag{12}$$

where J is the Jacobian matrix.

This method has an order of convergence equal to two (quadratic convergence), as long as an initial value close to the solution is known and $J^{-1}(\mathbf{x})$ exists. A weakness in the Newton-Raphson method arises from the need to calculate the Jacobian matrix $J(\mathbf{x})$ and to solve a linear system in each iteration to calculate its inverse $J^{-1}(\mathbf{x})$ [22].

In its implementation, direct calculation of $J^{-1}(\mathbf{x})$ and product $J^{-1}(\mathbf{x}_k) F(\mathbf{x}_k)$ can be avoided by solving the system $J(\mathbf{x}_k)\mathbf{s}_k = -F(\mathbf{x}_k)$ to determine the vector $\mathbf{s}_k$. Then, the new approximation $(\mathbf{x}_{k+1})$ is obtained by adding $\mathbf{s}_k$ to $\mathbf{x}_k$. This maneuver aims to reduce the computational cost required for each iteration [23]. The algorithm used is presented below.

Algorithm 1 Newton-Raphson Method

Require: Function $F(x)$; Jacobian matrix $J(x)$; initial approximation x_0; maximum number of iterations N; tolerance tol.
Ensure: Approximate method solution $x = (x_1, ..., x_n)^t$;
$error = tol + 1$; ▷ Set an initial error to enter the first while.
$k = 0$;
while $(tol < error)$ **do**
  Calculate $F(x_k)$ and $J(x_k)$;
  Solve $J(x_k)s = -F(x_k)$ to determine s;
  $s = -J(x_k)^{-1}F(x_k)$;
  $x_{k+1} = x_k + s$;
  $error = \left| x_{(k+1)} - x_{(k)} \right|$; ▷ Stop condition
  $x_k = x_{k+1}$; ▷ Update of x_k
  $k = k + 1$;
  if $k \geq N$ **then**
    To stop;
  end if
end while
Output (x_{k+1}); ▷ Solution found via Newton-Raphson method.

B. POTRA-PTÁK METHOD

In 1984, a method with order of convergence three (cubic) and an efficiency index higher than the Newton-Raphson method was presented in [41]. The basic idea consists of carrying out two evaluations (two-step method) of the given function, requiring only the calculation of first-order derivatives.

The Potra-Pták method can be described as follows:

$$\begin{aligned} \mathbf{y}_k &= \mathbf{x}_k - J^{-1}(\mathbf{x}_k) F(\mathbf{x}_k) \\ \mathbf{x}_{k+1} &= \mathbf{x}_k - J^{-1}(\mathbf{x}_k) \left[F(\mathbf{x}_k) + F(\mathbf{y}_k) \right]. \end{aligned} \tag{13}$$

Algorithm 2 Potra-Pták Method

Require: Function $F(x)$; Jacobian matrix $J(x)$; initial approximation x_0; maximum number of iterations N; tolerance tol.
Ensure: Approximate method solution $x = (x_1, ..., x_n)^t$;
$error = tol + 1$; ▷ Set an initial error to enter the first while.
$k = 0$;
while $(tol < error)$ **do**
  Calculate $F(x_k)$ and $J(x_k)$;
  $y_k = x_k - J(x_k)^{-1}F(x_k)$;
  Calculate $F(y_k)$;
  $x_{k+1} = x_k - J^{-1}(x_k)[F(x_k) + F(y_k)]$;
  $error = \left| x_{(k+1)} - x_{(k)} \right|$; ▷ Stop condition.
  $x_k \leftarrow x_{k+1}$; ▷ Update of x_k.
  $k = k + 1$;
  if $k \geq N$ **then**
    To stop;
  end if
end while
Output (x_{k+1}); ▷ Solution found via Potra-Pták method.

C. CHUN METHOD

The Chun method was presented in [24], where it was demonstrated to have an order of convergence equal to four. Furthermore, like the Potra-Pták method, it does not require calculations of order two derivatives. This method can be mathematically described as follows:

$$\begin{aligned} \mathbf{y}_k &= \mathbf{x}_k - J^{-1}(\mathbf{x}_k) F(\mathbf{x}_k) \\ \mathbf{x}_{k+1} &= \mathbf{x}_k - J^{-1}(\mathbf{x}_k) F(\mathbf{x}_k) - 2J^{-1}(\mathbf{x}_k) F(\mathbf{y}_k) + \\ &\quad \left[J^{-1}(\mathbf{x}_k) \right]^2 J(\mathbf{y}_k) F(\mathbf{y}_k) \ . \end{aligned} \tag{14}$$

The algorithm that illustrates the sequence of tasks to be performed by Chun's method is presented below.

D. FIGURES OF MERIT

To analyze the performance of an iterative method for nonlinear systems applied to grid impedance estimation, it is necessary to define which performance indicators will be evaluated. In this section, these indicators, referred to from now on as figures of merit, are described.

Algorithm 3 Chun Method

Require: Function $F(x)$; Jacobian matrix $J(x)$; initial approximation x_0; maximum number of iterations N; tolerance tol.
Ensure: Approximate method solution $x = (x_1, ..., x_n)^t$;
  $error = tol + 1$; ▷ Set an initial error to enter the first while.
  $k = 0$;
  while $(tol < error)$ **do**
    Calculate $F(x_k)$ and $J(x_k)$;
    $m_k = J(x_k)^{-1}F(x_k)$;
    $y_k = x_k - m_k$;
    Calculate $F(y_k)$ and $J(y_k)$;
    $n_k = J(x_k)^{-1}F(y_k)$;
    $x_{k+1} = x_k - m_k - 2n_k + J(x_k)^{-1}J(y_k)n_k$;
    $error = \left|x_{(k+1)} - x_{(k)}\right|$; ▷ Stop condition.
    $x_k = x_{k+1}$; ▷ Update of x_k.
    $k = k + 1$;
    if $k \geq N$ **then**
      To stop;
    end if
  end while
  Output (x_{k+1}); ▷ Solution found via Chun method.

1) Percentage Error

The percentage error (PE) represents the percentage difference between the actual value and the estimated value of the impedance of the grid. In this work, the percentage error referring to the grid resistance PE_R and the percentage error referring to the grid inductance PE_L are calculated as follows:

$$PE_R = \frac{R_g - R_{g-est}}{R_g} \times 100\% \tag{15}$$

$$PE_L = \frac{L_g - L_{g-est}}{L_g} \times 100\% \ , \tag{16}$$

where R_g is the actual grid resistance, R_{g-est} the estimated grid resistance, L_g the actual grid inductance and L_{g-est} the estimated grid inductance.

2) Execution Time

The execution time (ET), also known as runtime, represents the time (in seconds) that the implemented algorithm of the iterative method required after receiving the input stimuli to deliver the estimated values of the resistance and inductance of the grid.

3) Number of Iterations

The number of iterations (NI) represents the number of times that the algorithm implemented for a given iterative method needed to repeat its routine completely until it converged to a solution.

4) Efficiency Index

A very popular figure of merit in the comparison of iterative methods is the efficiency index (EI) [25]. This can be calculated as follows:

$$EI = \rho^{\frac{1}{a}} \ , \tag{17}$$

where ρ denotes the convergence order of the method and a means the number of function evaluations necessary to execute the method in each iteration.

According to [26], [27],

- for Newton-Raphson: $\rho = 2$ and $a = d + d^2$,
- for Potra-Pták: $\rho = 3$ and $a = 2d + d^2$,
- for Chun: $\rho = 4$ and $a = 2d + 2d^2$

evaluations for F and J. Here d represents the number of equations that make up the nonlinear system.

5) Computational Efficiency

Computational efficiency (CE) is also a common figure of merit applied to the context of analyzing performance of iterative methods,

$$CE = \rho^{\frac{1}{\gamma}} \ , \tag{18}$$

where γ represents the quantity of operations, measured in product units, required to perform each iteration, excluding the function evaluation computations.

As noted in [26], [27],

- for Newton-Raphson: $\gamma = d(d^2 + 3d - 1)/2$,
- for Potra-Pták: $\gamma = d(d^2 + 3d - 1)/2 + 2d^2$, and
- for Chun: $\gamma = d(d^2 + 3d - 1)/2 + 4d^2 + d$.

6) Computational Efficiency Index

The computational efficiency index (CEI) is a very robust figure of merit, as it takes into account the number of evaluations of scalar functions in each step of the iterative method, the number of evaluations of derived scalar functions and the number of products needed per iteration [28]. This metric is determined as follows:

$$CEI = \rho^{\frac{1}{\mathscr{C}}} \ , \tag{19}$$

where $\mathscr{C}$ is the computational cost per iteration. For

- Newton-Raphson: $\mathscr{C} = d(d^2 + 5d + 1)/2$,
- for Potra-Pták: $\mathscr{C} = d(d^2 + 9d + 3)/2$, and
- for Chun: $\mathscr{C} = d(d^2 + 15d + 5)/2$.

7) Stability

An iterative method is considered stable if minor variations in the data or initial conditions lead to only slight changes in the solution. Thus, an iterative method is labeled stable if

small alterations in the initial values lead to correspondingly small alterations in the final results; if not, it is termed unstable [29].

IV. RESULTS

To evaluate the performance of the iterative Newton-Raphson (NR), Potra-Pták (PP), and Chun (CH) methods applied to grid impedance estimation, the system represented in Fig. 3 was adopted. All parameters used are presented in Table 1.

The results presented in this section were obtained through real-time Model-In-the-Loop (mil) simulations. In this, the system model under analysis is embedded in the simulator (on its Central Processing Unit - cpu and/or Field Programmable Gate Array - FPGA), while the local machine (host) connected to the simulator is available for real-time interaction: changes to system component parameters (for example: controller gains) and visualization of results in real time. The OPAL-RT Technologies OP5700 simulator used

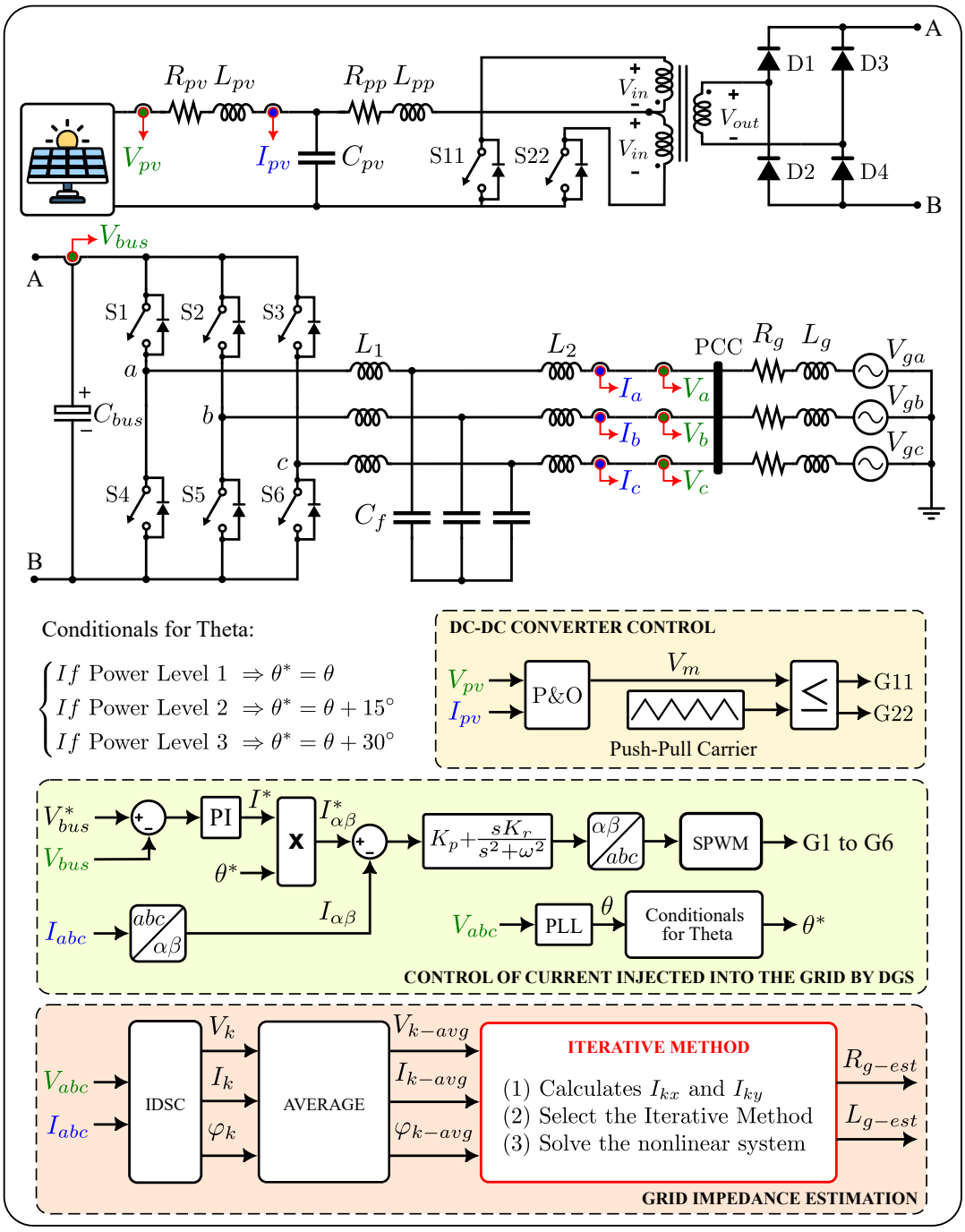

FIGURE 3. Complete schematic used to analyze the performance of iterative methods.

TABLE 1. System Parameters

Parameter	Value
Sun Irradiance	$1000\,\mathrm{W/m^2}$
Cell Tempeture	$25\,^{\circ}\mathrm{C}$
PV Module Model	Kyocera Solar KD325GX-LPB
Parallel Strings	3
Series-Connected Modules per String	2
Maximum PV Plant Power	1.95 kW
R_{pv} and L_{pv}	$1\,\mathrm{m\Omega}$ and $20\,\mu\mathrm{H}$
R_{pp} and L_{pp}	$1\,\mathrm{m\Omega}$ and $150\,\mu\mathrm{H}$
C_{pv}	$1150\,\mu\mathrm{F}$
V_{in} and V_{out}	230 V and 400 V
C_{bus}	$2250\,\mu\mathrm{F}$
Nominal DC Bus Voltage	400 V
L_1, L_2, and C_f	20 mH, 0.5 mH, and $5\,\mu\mathrm{F}$
R_g and L_g	$1\,\Omega$ and 1 mH
Nominal Line Voltage of the Grid	230 V
Nominal Grid Frequency	50 Hz
DC-DC Converter Carrier Frequency	60 kHz
MPPT Algorithm	Perturbation and Observation (P&O)
PI Proportional Gain	3
PI Integral Gain	40
K_p and K_r	27 and 7000
Carrier Frequency for SPWM	10 kHz
Fixed Step in Real Time	$1\,\mu\mathrm{s}$

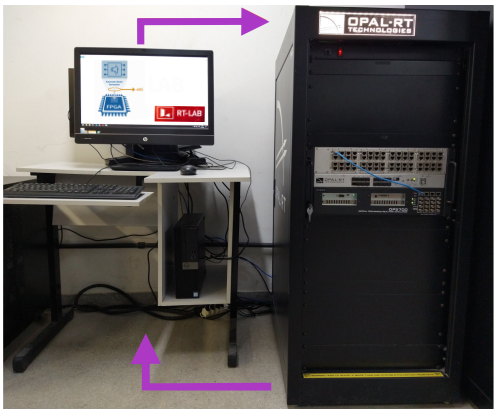

FIGURE 4. Real-time validation platform.

has an FPGA, two cpu, a system for conditioning up to 256 inputs/outputs, 16 fiber optic small form pluggable ports, and is designed to be used as a desktop or in a standard 19 inches rack. Operating with Virtex-7 FPGA, this simulator has two Intel Xeon E5-2667 @3.2 GHz cpu – each with 8 cores, an X10DRL-I-O motherboard and 32 GB of memory. The host-simulator configuration utilized is shown in Fig. 4.

The system presented in Fig. 3 consists of a photovoltaic (PV) plant connected to the grid through two conversion stages. The first stage consists of a DC-DC push-pull converter that introduces a gain in the voltage generated by the PV plant, in order to provide a voltage level suitable for the nominal value of the DC bus. A three-phase, three-leg inverter with two switches per leg and an LCL-type output filter interfaces with the grid, making up the DC-AC conversion stage. The grid is represented by a voltage source (V_{gabc}) in series with its resistance (R_g) and inductance (L_g).

The implemented control system can be basically divided into three blocks: the control dedicated to the DC-DC converter, the part responsible for controlling the levels of current injected into the grid, and the section designated for online estimation of the grid impedance via an iterative method.

To generate the gate signals G11 and G22 that control, respectively, the switches S11 and S22 that are part of the push-pull converter, the PV plant output voltage (V_{pv}), and current (I_{pv}) were measured, these values are the input of the maximum power point tracking (MPPT) method. A P&O (Perturbation and Observation) algorithm generates the reference signal (V_m), which, compared to a triangular carrier, results in switch gate signals.

The control system for the current injected into the grid has as input the measurements: the voltage in the PCC (V_{abc}), the current injected into the grid (I_{abc}) and the voltage at the DC bus (V_{bus}). The adopted grid impedance estimation method requires successive injection of three different power levels into the grid. To meet this demand, successive variations were programmed in the DC bus voltage reference signal (V^*_{bus}) and in the reference phase angle (θ^*) for the current injected into the grid.

A phase-locked loop (PLL) delivers the θ angle to the block called *Conditionals for Theta*. This adjusts the θ values based on the current power level, resulting in the reference angle θ^* for the current injected into the grid. The θ angle adjustment process boils down to the following:
if Power Level 1 $\Rightarrow$ $\theta^* = \theta$;
if Power Level 2 $\Rightarrow$ $\theta^* = \theta + 15°$;
if Power Level 3 $\Rightarrow$ $\theta^* = \theta + 30°$.

The reference signal for the DC bus voltage V^*_{bus} varies according to the following conditions:
if Power Level 1 $\Rightarrow$ V^*_{bus} = 1.00 $\times$ Nominal DC bus voltage;
if Power Level 2 $\Rightarrow$ V^*_{bus} = 1.50 $\times$ Nominal DC bus voltage;
if Power Level 3 $\Rightarrow$ V^*_{bus} = 1.25 $\times$ Nominal DC bus voltage.

The voltage measured on the DC bus (V_{bus}) is compared with its reference value, and the resulting error is processed by a PI controller, generating the reference amplitude for the current I^*. The reference angle θ^* combined with I^* makes up the reference current ($I^*_{\alpha\beta}$) on the $\alpha\beta$ axes. The current injected into the grid (I_{abc}) is measured and transformed to the $\alpha\beta$ reference, becoming $I_{\alpha\beta}$. The error resulting from the comparison of $I^*_{\alpha\beta}$ with $I_{\alpha\beta}$ is processed by a resonant controller. The resulting signal is taken back to the stationary reference frame where it serves as a reference for a sinusoidal pulse width modulation scheme (SPWM). The gate signals G1 to G6 control the inverter switches from S1 to S6, thus controlling the current injected into the grid.

The control block dedicated to estimating the grid impedance has as input the voltage measured at the PCC and the current injected into the grid. An instantaneous decompo-

sition into sequence components (IDSC) algorithm estimates the voltage amplitude at the PCC (V_k), the amplitude of the current injected into the grid (I_k) and the phase angle of this current (φ_k) for each power level imposed by the control system. Consequently, for each level of power injected into the grid, there is a set of 3 estimated values: [V_1 I_1 φ_1], [V_2 I_2 φ_2], and [V_3 I_3 φ_3], for power levels 1, 2 and 3, respectively.

The values of these estimates, in general, fluctuate around a certain value. Therefore, a block called *Average* was built, which is responsible for taking the arithmetic average of the last 2500 samples contained at the end of the duration time interval for each of the three power levels. The average values of these sections of V_k, I_k and φ_k are the input of the block that contains the iterative methods under analysis.

Note that the block containing the iterative method should only be activated after the end of the time interval of the third level of power injected into the grid, as only after this instant will the three sets of estimated values become available necessary to solve the nonlinear system that models the problem.

With the three sets of necessary input values, the block containing the iterative method (Newton-Raphson, Potra-Pták, or Chun) separates the real and imaginary parts of the current phasor $I_k\angle\varphi_k$. From there, the system can estimate the impedance of the grid by solving the nonlinear system of equations (10). As a result, the estimated grid resistance (R_{g-est}) and the estimated grid inductance (L_{g-est}) are obtained.

To analyze the performance of the iterative methods, an observation window with a total duration of 1.6 seconds was established. Within this time interval, the three different power levels required and imposed via the control system are distributed as shown in Table 2. The results obtained are presented in Fig. 5 and Fig. 6.

The results shown in Fig. 5(a) and Fig. 5(b), show the measured output voltage (V_{pv}) and current (I_{pv}) of the PV plant. Of these, an average power supply of around 1.73 kW was observed.

The voltage measured on the DC bus (V_{bus}) during the section referring to the first power level remained at 400 V (nominal value). After imposing the second power level by changing V^*_{bus} to 600 V, a transient lasting 0.3 s was observed until entry into the steady state. At 0.6 s, the third power level started, V^*_{bus} was changed to 500 V, and the DC bus voltage took again 0.3 s to reach its reference value. This behavior is shown in Fig. 5(c).

Fig. 5(d) shows the action of the *Conditionals for Theta* block on the phase angle delivered by the PLL. It can be seen that, although the value of θ does not vary throughout

TABLE 2. Duration interval of each power level imposed

Power Level	Value	Duration Range (in seconds)
1	100% × Nominal Power	From 0 to 0.2
2	95% × Nominal Power	From 0.2 to 0.6
3	110% × Nominal Power	From 0.6 to 1

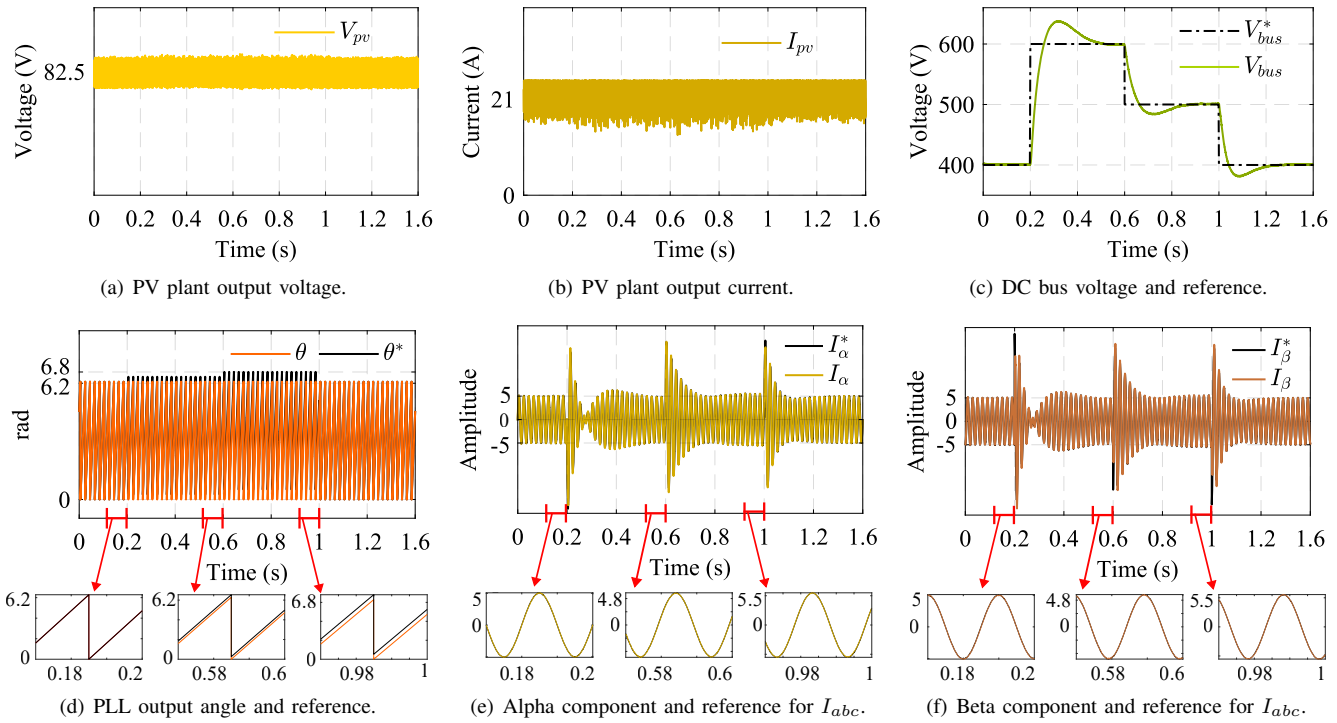

(a) PV plant output voltage.

(b) PV plant output current.

(c) DC bus voltage and reference.

(d) PLL output angle and reference.

(e) Alpha component and reference for I_{abc}.

(f) Beta component and reference for I_{abc}.

FIGURE 5. Results obtained for the system under analysis - Block 1.

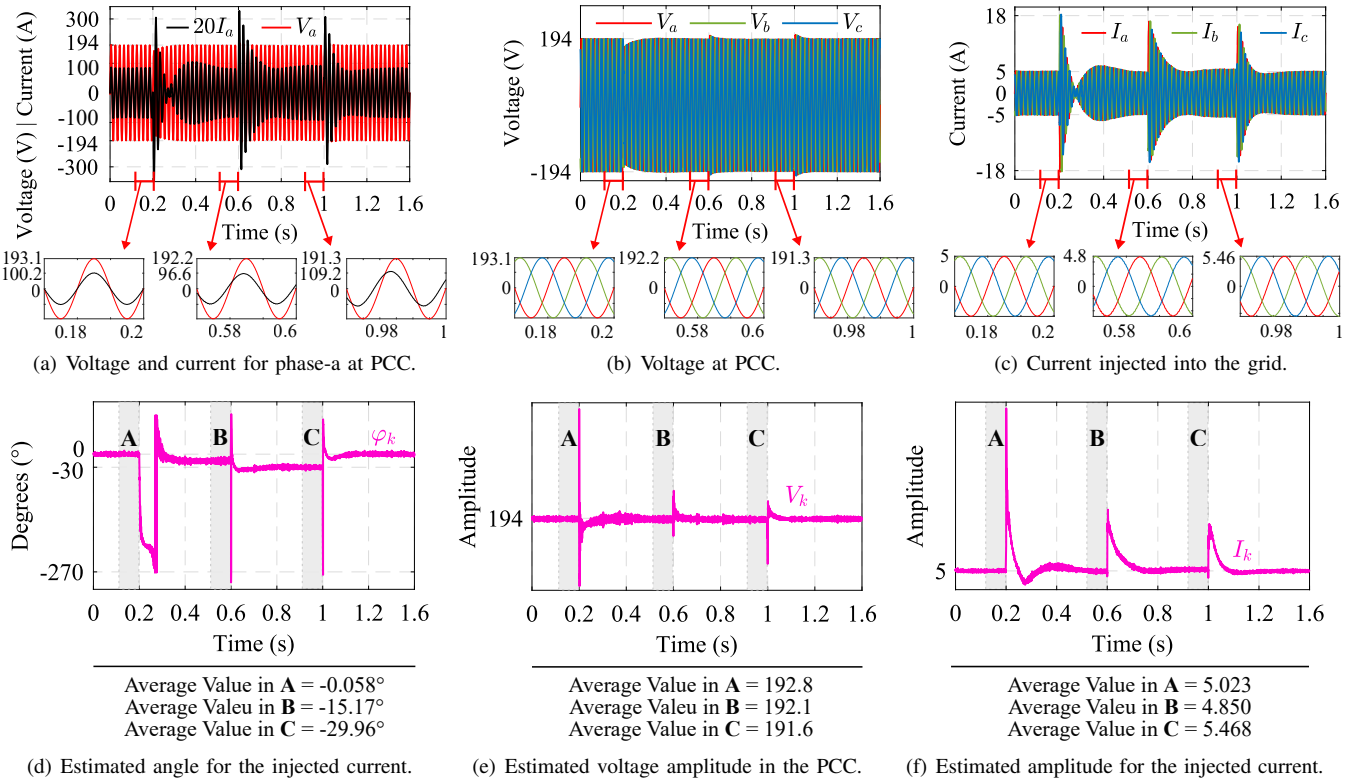

(a) Voltage and current for phase-a at PCC.
(b) Voltage at PCC.
(c) Current injected into the grid.
(d) Estimated angle for the injected current.
(e) Estimated voltage amplitude in the PCC.
(f) Estimated amplitude for the injected current.

FIGURE 6. Results obtained for the system under analysis - Block 2.

the observation window, the value of the reference angle θ^* delivered to the control system varies according to each different level of power injected into the grid.

The results presented in Figs. 5(e) and 5(f) show that for both the α axis and the β axis, the components of the current injected into the grid followed their reference signals during all imposed power levels.

The consequence of the variation in the θ^* reference angle on the current injected into the grid is shown for phase-a in Fig. 6(a). It is noted that for the first power level (nominal), the voltage and current in the PCC are in phase, that is, the unity power factor. In the time periods referring to the second and third power levels, it was observed that the current and voltage are out of phase with each other; however, this behavior was imposed on purpose to meet the need for the impedance estimation method.

The variations in power injected into the grid become explicit when observing the variations in voltage levels at the PCC and current injected into the grid. These signals were recorded and are presented in Figs. 6(b) and 6(c), for the voltage at the PCC and for the injected current, respectively.

Figs. 6(d), 6(e) and 6(f) present the results of applying the IDSC algorithm throughout the observation window. Of these, it was observed that after imposing a new power level, the algorithm faces a transition period until it converges to an estimate. The longest observed transient period was recorded for I_k after the transition from power level one to two, where it took 0.3 s to stabilize. These periods depend entirely on the dynamics of the system and are practically equal to the periods necessary to stabilize the input variables of the IDSC technique.

In Fig. 6(d) it was observed that, as programmed, the angle of the current injected into the grid (φ_k) varied according to the conditions imposed through the control system, assuming pre-established values in each section of power. The estimated amplitude for the PCC voltage shown in Fig. 6(e) presented relatively small variations, sufficient to meet the demands of the impedance estimation method. From Fig. 6(f) we can see the variation in the estimated amplitude for the injected current (I_k) proportional to the power levels proposed in Table 2.

Furthermore, 6(d), 6(e) and 6(f) show the action zone of the *Average block*, which is highlighted at the end of the duration interval of each of the three different power levels imposed by the control system. Respectively, zones **A**, **B**, and **C** refer to the last 2500 samples recorded at the end of the time interval of power levels one, two, and three.

From the instant of time equal to one second, the system collected and stored the necessary set of input values [V_1 I_1 φ_1 V_2 I_2 φ_2 V_3 I_3 φ_3] to estimate the grid impedance via an iterative method

In this work, the performance of the Newton-Raphson (NR), Potra-Pták (PP), and Chun (CH) methods applied to grid impedance estimation is compared taking into account

the following figures of merit: Percentage Error (PE), Execution Time (ET), Number of Iterations (NI), Efficiency Index (EI), Computational Efficiency (CE), Computational Efficiency Index (CEI), and Stability (STB). The results obtained are presented in Tables 3 and 4.

To compare the iterative methods, equality conditions were implemented, highlighting that all the iterative methods evaluated started from the same initial solution, this solution being: $\mathbf{x}_0 = [0.1\ 0.1\ 0.1\ 0.1\ 0.1\ 0.1\ 0.1\ 0.1]^{\mathrm{T}}$, also, all were programmed with a tolerance equal to 0.1.

In addition to the results obtained for the parameters contained in Table 1, results were also recorded by changing the grid inductance to L_g = 1.5 mH. When successively repeated applications of iterative methods to solve the same system, for computational reasons, the performance for the figures of merit, PE and ET may vary slightly with each different test. Therefore, in this work, the values presented for these indicators are the average value obtained after ten rounds of successive tests.

According to the results grouped in Table 3, it is observed that the highest percentage error in estimating grid resistance (PE_R) was recorded for the PP method. The method that obtained the lowest PE_R was the CH method. Regarding the percentage error in estimating the grid inductance (PE_L), what was observed for PE_R was repeated.

The lowest ETs were obtained via NR; in this regard, PP was inferior to both NR and the CH method. Regarding the number of iterations needed to converge to the estimated value, NR and PP needed 14 iterations, while CH used 25 iterations when L_g = 1 mH and 24 iterations when L_g = 1.5 mH.

The figures of merit EI, CE and CEI depend on the number of equations that make up the system under analysis, the order of convergence of the iterative method, the number of operations performed per iteration, and the number of function and Jacobian evaluations per iteration. These indicators were calculated according to (17), (18) and (19), the results are presented in Table 4.

As the PP and CH methods (as well as most iterative methods) derive from the NR method, the values obtained for EI, CE and CEI are very similar for the three methods under analysis. However, pragmatically, in these aspects, the PP method is slightly superior to the others.

To conclude on the stability of the iterative methods analyzed, successive tests were carried out in which the values that make up the initial solution vector were changed by $\pm 50\%$. During this test battery, it was observed that small variations in this vector also imply small variations in the estimated impedance values. Therefore, all methods were classified as stable when applied specifically to this problem.

V. CONCLUSION

In this work, a comparative study was presented to evaluate the performance of iterative methods for nonlinear systems applied to grid impedance estimation. Newton-Raphson (NR), Potra-Pták (PP), and Chun (CH) methods were incorporated into the control system of a grid-connected photovoltaic plant for the purpose of estimating the resistance and inductance parameters of the grid. This analysis aimed to contribute to the process of selecting the most appropriate iterative method to be used in applications that require grid impedance estimates.

The percentage error (PE), execution time (ET), number of iterations (NI), efficiency index (EI), computational efficiency (CE), computational efficiency index (CEI), and stability (STB) were the indicators of adoption performance.

Real-time simulations demonstrated the effectiveness of the adopted estimation technique, as well as proving the applicability of iterative methods for online estimation of grid parameters.

From the results obtained, it is possible to conclude that in relation to PE, the CH method performed better than the others. With regard to ET, it was observed that the difference between the average ET values for the NR and CH methods is only 5 ms. Taking into account that the estimated value delivered to a given application is fundamental for the assertiveness of the control action to be taken, it is concluded

TABLE 3. Performance results of iterative methods applied to grid impedance estimation - Figures of Merit: Block 1.

Figure of Merit	Newton-Raphson (NR)		Potra-Pták (PP)		Chun (CH)	
	When $L_g = 1\,\mathrm{mH}$	When $L_g = 1.5\,\mathrm{mH}$	When $L_g = 1\,\mathrm{mH}$	When $L_g = 1.5\,\mathrm{mH}$	When $L_g = 1\,\mathrm{mH}$	When $L_g = 1.5\,\mathrm{mH}$
Percentage Error for R_{g-est} (PE_R)	0.031602%	0.038923%	0.368153%	0.375474%	0.015155%	0.009297%
Percentage Error for L_{g-est} (PE_L)	0.131378%	0.081931%	0.931425%	0.615296%	0.063004%	0.019570%
Execution Time (ET)	24.98 ms	18.28 ms	41.86 ms	34.57 ms	26.99 ms	27.82 ms
Number of Iterations (NI)	14	14	14	14	25	24

TABLE 4. Performance results of iterative methods applied to grid impedance estimation - Figures of Merit: Block 2.

Figure of Merit	Newton-Raphson (NR)	Potra-Pták (PP)	Chun (CH)
Efficiency Index (EI)	1.0096	1.0138	1.0096
Computational Efficiency (CE)	1.0019	1.0023	1.0022
Computational Efficiency Index (CEI)	1.0012	1.0019	1.0018
Stability	Yes	Yes	Yes

that the Chun method is more suitable for applications that require great precision of estimates, such as, for example, guaranteeing stability. For applications that require reasonable precision (when compared to that provided by the CH method) and the speed of decision making by the control system is paramount, the NR method is more appropriate. An example of this type of application being anti- islanding detection.

ACKNOWLEDGMENT

The authors express their gratitude to the Paraiba State Research Foundation (FAPESQ) through Grant 019/2023, as well as the Coordination for the Improvement of Higher Education Personnel (CAPES), for their financial backing of this study. Additionally, thanks are extended to the National Council for Scientific and Technological Development (CNPq) under process numbers 313855/2021-8.

AUTHOR'S CONTRIBUTIONS

DE ASSIS, J. R. P.: Conceptualization, Data Curation, Formal Analysis, Investigation, Methodology, Software, Validation, Visualization, Writing – Original Draft, Writing – Review & Editing. **GOMES, A. S.**: Conceptualization, Data Curation, Formal Analysis, Investigation, Methodology, Software, Writing – Original Draft. **GOMES, H. M. T. C.**: Conceptualization, Formal Analysis, Investigation, Methodology. **COSTA, F. F.**: Conceptualization, Formal Analysis, Investigation, Methodology. **FELIPE, W. F.**: Conceptualization, Formal Analysis, Investigation, Methodology. **CORRÊA, M. B. R.**: Conceptualization, Data Curation, Formal Analysis, Investigation, Methodology, Project Administration, Supervision, Writing – Review & Editing. **FERNANDES, D. A.**: Conceptualization, Data Curation, Formal Analysis, Funding Acquisition, Investigation, Methodology, Project Administration, Resources, Supervision, Writing – Review & Editing.

PLAGIARISM POLICY

This article was submitted to the similarity system provided by Crossref and powered by iThenticate – Similarity Check.

REFERENCES

[1] International Energy Agency - IEA, "The Evolution of Energy Efficiency Policy to Support Clean Energy Transitions", Digital Format, December 2023, URL: https://www.iea.org/reports/the-evolution-of-energy-efficiency-policy-to-support-clean-energy-transitions.

[2] T. B. Hadj, A. Ghodbane, E. B. Mohamed, A. A. Alfalih, "The transition to renewable energy through financial development and under natural resources threshold in emerging countries", *Environment, Development and Sustainability*, Jan 2024, doi:10.1007/s10668-023-04389-1, URL: https://doi.org/10.1007/s10668-023-04389-1.

[3] R. D. Middlebrook, S. Cuk, "A general unified approach to modelling switching-converter power stages", *in 1976 IEEE Power Electronics Specialists Conference*, pp. 18–34, 1976, doi:10.1109/PESC.1976.7072895.

[4] S. Hiti, D. Boroyevich, "Small-signal modeling of three-phase PWM modulators", *in PESC Record. 27th Annual IEEE Power Electronics Specialists Conference*, vol. 1, pp. 550–555 vol.1, 1996, doi:10.1109/PESC.1996.548634.

[5] H. Mao, D. Boroyevich, F. Lee, "Novel reduced-order small-signal model of a three-phase PWM rectifier and its application in control design and system analysis", *IEEE Transactions on Power Electronics*, vol. 13, no. 3, pp. 511–521, 1998, doi:10.1109/63.668114.

[6] F. Blaabjerg, Z. Chen, S. Kjaer, "Power electronics as efficient interface in dispersed power generation systems", *IEEE Transactions on Power Electronics*, vol. 19, no. 5, pp. 1184–1194, 2004, doi:10.1109/TPEL.2004.833453.

[7] M. Liserre, R. Teodorescu, F. Blaabjerg, "Stability of photovoltaic and wind turbine grid-connected inverters for a large set of grid impedance values", *IEEE Transactions on Power Electronics*, vol. 21, no. 1, pp. 263–272, 2006, doi:10.1109/TPEL.2005.861185.

[8] M. K. De Meerendre, E. Prieto-Araujo, K. H. Ahmed, O. Gomis-Bellmunt, L. Xu, A. Egea-Àlvarez, "Review of Local Network Impedance Estimation Techniques", *IEEE Access*, vol. 8, pp. 213647–213661, 2020, doi:10.1109/ACCESS.2020.3040099.

[9] N. Mohammed, T. Kerekes, M. Ciobotaru, "An Online Event-Based Grid Impedance Estimation Technique Using Grid-Connected Inverters", *IEEE Transactions on Power Electronics*, vol. 36, no. 5, pp. 6106–6117, 2021, doi:10.1109/TPEL.2020.3029872.

[10] R. L. d. A. Ribeiro, A. Oshnoei, A. Anvari-Moghaddam, F. Blaabjerg, "Adaptive Grid Impedance Shaping Approach Applied for Grid-Forming Power Converters", *IEEE Access*, vol. 10, pp. 83096–83110, 2022, doi:10.1109/ACCESS.2022.3196921.

[11] H. M. T. C. Gomes, L. L. O. Carralero, J. H. Suárez, A. P. N. Tahim, J. R. Pinheiro, F. F. Costa, "Estimativa de Impedância para Suporte de Estabilidade e Qualidade de Energia em Inversores Conectados à Rede", *Eletrônica de Potência*, vol. 27, no. 2, p. 165–176, Jun. 2022, doi:10.18618/REP.2022.2.0004, URL: https://journal.sobraep.org.br/index.php/rep/article/view/67.

[12] A. Suarez, C. Blanco, P. Garcia, A. Navarro-Rodriguez, J. Manuel Cano Rodriguez, "Grid Impedance Estimator for Active Multisource AC Grids", *IEEE Transactions on Smart Grid*, vol. 14, no. 3, pp. 2023–2033, 2023, doi:10.1109/TSG.2022.3212770.

[13] D. O. Cardoso, H. M. T. C. Gomes, F. A. d. C. Bahia, A. P. N. Tahim, J. R. Pinheiro, F. F. Costa, "Impacto do PLL para Estimação de Impedância de Rede e Avaliação de Estabilidade no Domínio DQ em Sistemas com Inversores Conectados", *Eletrônica de Potência*, vol. 28, no. 2, p. 107–118, Mar. 2023, doi:10.18618/REP.2023.2.0050, URL: https://journal.sobraep.org.br/index.php/rep/article/view/12.

[14] J. Mace, A. Cervone, D. Dujic, "Self-Synchronized Grid Impedance Estimation Unit Using Interpolated DFT Technique", *IEEE Transactions on Power Electronics*, vol. 39, no. 4, pp. 4624–4635, 2024, doi:10.1109/TPEL.2023.3342317.

[15] Y. Cheng, W. Wu, Y. Yang, E. Koutroulis, H. S.-H. Chung, M. Liserre, F. Blaabjerg, "Zero-Sequence Voltage Injection-Based Grid Impedance Estimation Method for Three-Phase Four-Wire DC/AC Grid-Connected Inverter", *IEEE Transactions on Industrial Electronics*, vol. 71, no. 7, pp. 7273–7279, 2024, doi:10.1109/TIE.2023.3306395.

[16] J. R. P. De Assis, A. Da Silva Gomes, H. M. T. Cotrim Gomes, F. F. Costa, W. F. Felipe, M. B. De Rossiter Corrêa, D. A. Fernandes, "Performance of Parametric Methods for Online Grid-Impedance Estimation Applied to PV Systems", *in 2023 IEEE 8th Southern Power Electronics Conference and 17th Brazilian Power Electronics Conference (SPEC/COBEP)*, pp. 1–6, 2023, doi:10.1109/SPEC56436.2023.10407902.

[17] D. A. Fernandes, S. R. Naidu, C. Coura, "Instantaneous Sequence-Component Resolution of 3-Phase Variables and Its Application to Dynamic Voltage Restoration", *IEEE Transactions on Instrumentation and Measurement*, vol. 58, no. 8, pp. 2580–2587, 2009, doi:10.1109/TIM.2009.2015634.

[18] J. Taylor, *Classical Mechanics*, G - Reference,Information and Interdisciplinary Subjects Series, University Science Books, 2005, URL: https://books.google.com.br/books?id=P1kCtNr-pJsC.

[19] E. L. Allgower, K. Georg, *et al.*, *Computational solution of nonlinear systems of equations*, vol. 26, American Mathematical Soc., 1990.

[20] I. Argyros, *Computational Theory of Iterative Methods*, vol. 15, Elsevier Science, 2007.

[21] J. Hueso, E. Martínez, J. Torregrosa, "Third and fourth order iterative methods free from second derivative for nonlinear systems", *Applied Mathematics and Computation*, vol. 211, pp. 190–197, 05 2009, doi:10.1016/j.amc.2009.01.039.

[22] B. Polyak, "Newton's method and its use in optimization", *European Journal of Operational Research*, vol. 181, no. 3, pp. 1086–

1096, 2007, doi:https://doi.org/10.1016/j.ejor.2005.06.076, URL: https://www.sciencedirect.com/science/article/pii/S0377221706001469.

[23] R. L. Burden, J. D. Faires, *Numerical Analysis*, Cengage Learning, 2011.

[24] C. Chun, "A new iterative method for solving nonlinear equations", *Applied Mathematics and Computation*, vol. 178, no. 2, pp. 415–422, 2006, doi:https://doi.org/10.1016/j.amc.2005.11.055, URL: https://www.sciencedirect.com/science/article/pii/S0096300305009860.

[25] G. Optiz, "A. M. Ostrowski (University of Basel), Solution of Equations and Systems of Equations (Vol. 9 of Pure and Applied Mathematics). IX + 202 S. New York and London 1960. Academic Press. Preis geb. $ 6.80", *ZAMM - Journal of Applied Mathematics and Mechanics / Zeitschrift für Angewandte Mathematik und Mechanik*, vol. 43, no. 1-2, pp. 89–89, 1963, doi:https://doi.org/10.1002/zamm.19630430112, URL: https://onlinelibrary.wiley.com/doi/abs/10.1002/zamm.19630430112, https://onlinelibrary.wiley.com/doi/pdf/10.1002/zamm.19630430112.

[26] A. Cordero, J. Hueso, E. Martínez, J. Torregrosa, "A modified Newton-Jarratt's composition", *Numerical Algorithms*, vol. 55, pp. 87–99, 09 2010, doi:10.1007/s11075-009-9359-z.

[27] A. Cordero, J. L. Hueso, E. Martínez, J. R. Torregrosa, "Increasing the convergence order of an iterative method for nonlinear systems", *Applied Mathematics Letters*, vol. 25, no. 12, pp. 2369–2374, 2012, doi:https://doi.org/10.1016/j.aml.2012.07.005, URL: https://www.sciencedirect.com/science/article/pii/S0893965912003369.

[28] M. Grau-Sánchez, Àngela Grau, M. Noguera, "On the computational efficiency index and some iterative methods for solving systems of nonlinear equations", *Journal of Computational and Applied Mathematics*, vol. 236, no. 6, pp. 1259–1266, 2011, doi:https://doi.org/10.1016/j.cam.2011.08.008, URL: https://www.sciencedirect.com/science/article/pii/S037704271100447X.

[29] A. Cordero, J. M. Gutierrez, A. A. Magrenan, J. R. Torregrosa, "Stability analysis of a parametric family of iterative methods for solving nonlinear models", *Applied Mathematics and Computation*, vol. 285, pp. 26–40, 2016, doi:https://doi.org/10.1016/j.amc.2016.03.021, URL: https://www.sciencedirect.com/science/article/pii/S0096300316302144.

BIOGRAPHIES

Jefferson Rafael Pereira de Assis received his bachelor's degree (2019) and master's degree (2021) in Electrical Engineering from the Federal University of Paraíba. He is currently a Ph.D. student in Electrical Engineering at the Federal University of Campina Grande. His research interests include applications of power electronics in distribution systems, power quality, integration of renewable energy, grid impedance estimation techniques, and stability of grid-connected converters. He is a student member of the Brazilian Power Electronics Association (SOBRAEP) and Institute of Electrical Engineering and Electronics (IEEE).

Andréia da Silva Gomes received a bachelor's degree (2021) in electrical engineering from the Federal University of Campina Grande and a master's degree (2024) in electrical engineering from the Federal University of Paraíba. She is currently a Ph.D. student in electrical engineering at the Federal University of Bahia. Her research interests include distributed generation, integration of renewable energy sources, electrical installations, electrical power systems, energy quality, and electrotechnical projects.

Hugo Matheus Teixeira Cotrim Gomes received his bachelor's degree (2010), master's degree (2016), and Ph.D. (2022) in Electrical Engineering from the Federal Institute of Bahia and the Federal University of Bahia, respectively. His research topics include control in distributed generation systems, PLL, grid impedance estimation techniques, and stability study.

Fabiano Fragoso Costa holds a degree in Engineering Electrical from the University of São Paulo (1997), master's degree in Electrical Engineering from the Federal University of Campina Grande (2001) and Ph.D. in Electrical Engineering from Federal University of Campina Grande (2005). Realized postdoctoral research at CPES (Center for Power Electronics Systems) at Virginia Tech (USA). He is currently a professor associate at the Federal University of Bahia in the Department of Electrical Engineering. His research interests include topics related to modeling switched converters through impedance techniques; systems stability interconnected switches in the frequency domain, with emphasis on grid-connected LCL inverters; methods phase capture loop synchronization (PLLs) and electrical grid impedance estimation techniques. He is a member of the Brazilian Power Electronics Association (SOBRAEP) and a Senior Member of the Institute of Electrical Engineering and Electronics (IEEE).

Wellington Ferreira Felipe received a bachelor's degree in Electrical Engineering from the Federal University of Campina Grande (2007) and a master's degree in Electrical Engineering from the Federal University of Paraíba (2023). He is currently a higher level III professional at Eletrobras-Chesf. He has experience in the area of Electrical Engineering with an emphasis on Electrical Energy Generation, working mainly on the following topics: Measurement, Protection, Command, Control and Supervision of Substations (MPCCS), modernization of hydroelectric plants, photovoltaic systems, and power electronics. He is a student member of the Brazilian Power Electronics Association (SOBRAEP).

Maurício Beltrão de Rossiter Corrêa received the titles Electrical Engineer, Master and Doctor in Electrical Engineering at the Federal University of Paraíba, Campina Grande, Brazil, respectively, in 1996, 1997 and 2002. From 1997 to 2004, he was at the Federal Education Center Technology of Alagoas, Brazil. From 2001 to 2002, he did an internship at Wisconsin Electric Machines and Power Electronics Consortium (WEMPEC), at the University of Wisconsin, Madison, WI, USA as part of the PhD program. From 2004 to 2024, he worked in the Electrical Engineering Department of the Federal University of Campina Grande, Campina Grande. He is currently a professor at the Federal University of Alagoas. He was deputy general coordinator of the "The 2005 IEEE Power Electronics Specialists Conference"(PESC 2005) and the IEEE International Future Topic (B) Coordinator Energy Challenge 2011 (IFEC 2011). Your interests research include drive systems, power electronics, and renewable energy.

Darlan Alexandria Fernandes received the B.S. degree in electrical engineering from the Federal University of Paraiba, Brazil, in 2002, and the M.S. and Ph.D. degrees in electrical engineering from the Federal University of Campina Grande, Brazil, in 2004 and 2008, respectively. He was a Visiting Scholar at the Center for Power Electronics Systems (CPES) at the Virginia Polytechnic Institute and State University (Virginia Tech), Blacksburg, United States, from 2018 to 2019. From 2007 to 2011, he was a Professor with the Industry Department in the Federal Center of Technological Education of Rio Grande do Norte. He is currently an Associate Professor with the Department of Electrical Engineering, Federal University of Paraiba, Brazil. His research interests are in the applications of power electronics in distribution systems, power quality, photovoltaic systems, and impedance-based control design techniques for static converters. He is a member of the Brazilian Power Electronics Association (SOBRAEP) and IEEE.